Multiple-scattering x-ray-absorption fine-structure analysis and thermal expansion of alkali halides

A. I. Frenkel
School of Physics and Astronomy, Tel Aviv University, Ramat Aviv 69978, Israel

E. A. Stern, M. Qian, and M. Newville
Department of Physics, University of Washington, Seattle, Washington 98195
(Received 16 February 1993)

X-ray-absorption fine-structure (XAFS) data of RbBr, RbCl, and KBr at 30 K and 125 K were measured and analyzed. An ionized-atom multiple-scattering calculation and a correlated Debye model were used for fitting the theory used in the FEFF5 computer code to data. The modifications of FEFF5 necessary to obtain good fits to the data are discussed. The results demonstrate the domination of single-scattering and focusing paths in XAFS and the determination of vibrational information through at least 10 Å around the center atom. Numerical calculations were performed to analyze the cause of the difference found between the forward-scattering amplitudes of Rb^+ and Br^- focusing atoms. The second and third cumulants were determined of the first and second neighbors and were used to calculate the temperature dependence of the thermal-expansion coefficient including quantum effects at low temperature. Agreement with macroscopic thermal-expansion measurements was found.

I. INTRODUCTION

The x-ray-absorption fine-structure (XAFS) technique has been applied for about 20 years to determine the partial pair correlation function of atoms in both crystalline and noncrystalline samples. It has the advantage of directly observing the local structure around specific atoms. The local structure is probed by the photoelectrons excited from those atoms absorbing the x rays. For the first few neighbors, the photoelectron contribution to the XAFS is dominated by single scattering (SS). Because of the relative simplicity with which this SS can be interpreted, most of the applications of XAFS to date have concentrated on determining the local structure of the first neighbors.

With development of an accurate theory and its computer code[1,2] FEFF5 that can include multiple-scattering (MS) effects with great efficiency, the use of XAFS to determine structure information beyond the first or second neighbors has become very feasible. One way FEFF5 attains this efficiency is to presort the MS paths, and to retain only those that are significant. Combining FEFF5 with a routine that fits in R space instead of k space the total path length is limited by the maximum R value to be fitted, which then limits the paths required to an easily manageable number. This combination reduces the computing requirements dramatically so that the structural parameters can be rapidly determined using just microcomputers. Some of the potential of the applications this opens up has been illustrated using a less accurate theory to investigate the local structure about the Nb atom in $K(Ta_{1-x}Nb_x)O_3$ both below and above the ferroelectric transition.[3] Preliminary results on ferroelectric $PbTiO_3$ have recently also been reported[4,5] using FEFF5. Both these analyses show that the local distortions that cause the electric dipole moments in the ferroelectric state persist in the paraelectric phase; i.e., the average structure as determined by diffraction is quite different than the actual local structure.

In this paper we perform a detailed investigation and evaluation of FEFF5 for analyzing the XAFS of the ionic salts RbBr, KBr, RbCl. We find that the ionized-atom potentials of FEFF5, with suitable corrections, are quite adequate to permit the determination of accurate structural information in these salts. In particular, accurate thermal vibration information is obtained out to the seventh nearest neighbor. It should be emphasized that if the structure is unknown XAFS can typically refine the structure only up to about four neighboring shells of atoms,[6] but in the case discussed here the crystal structure (i.e., the average structure) is known and then some further structural information can be ascertained out to larger distances. These salts, particularly RbBr, have significant anharmonicity in their vibrations, even below room temperature. The XAFS analysis accurately quantifies this anharmonicity and shows good agreement between the atomic scale measurements and macroscopic thermal expansion.

An outline of the paper is as follows. In Sec. II the experimental details are presented. Sections III and IV discuss details of fitting the theory to the measurements. The results of the fits are presented in Sec. V. A discussion of the atomic characteristics that are most important in causing enhancement of the forward-scattering amplitude in Rb and Br is presented in Sec. VI, while the analyses of thermal expansion from atomic scale measurements are discussed in Sec. VII. Section VIII emphasizes some physical constraints that must be satisfied by the XAFS

0163-1829/93/48(17)/12449(10)/$06.00

analysis. A summary and conclusion are presented in Sec. IX.

II. EXPERIMENT

The samples used in this work were all powders. High purity (99.9% or better) materials of RbBr, KBr, and RbCl were supplied by Alfa (Johnson Matthey). All these materials are very hygroscopic; therefore, the raw chemicals were first heated to 393 K for an hour to remove any moisture and then the sample preparation was performed using a dry box. While in the dry box the samples were sealed in a vacuum tight cell with kapton windows and indium seals. The sealed samples were stored in a vacuumed desiccator until use.

Care was taken to ensure high quality XAFS measurements. To avoid the sample thickness effect,[7] it is required that the following condition be satisfied (for concentrated materials):

$$\Delta\mu x \leq 1,$$

where $\Delta\mu x$ is the edge step. The corresponding maximum thicknesses for RbBr, KBr, and RbCl are 50 μm (both Rb and Br edge), 44 μm (Br edge), and 50 μm (Rb edge), respectively.

It is also important that the size of the particles be smaller than one absorption length in the material,[8] $\mu d < 1$, where d is the particle size and μ is the total absorption coefficient. Thus, d should be smaller than μ^{-1}. For the materials used in this work, $d \leq 25$ μm. The particle size of the commercial raw materials was too large and nonuniform, and a grinding and sieving treatment through 400 mesh in the dry box was done. After this treatment the resultant powder was rubbed on to Scotch tape, and the excess powder was removed. It was found that 14–20 layers of tape were required to obtain a total $\Delta\mu x \approx 1$. Under these conditions the thickness effect distortions are expected to be negligible.[7]

The XAFS measurements were performed on beamline X-11A at NSLS using a double crystal (111) silicon monochromator. Due to the high anharmonicity of these materials, low temperature measurements were necessary and they were taken using a Displex refrigeration system. The higher x-ray harmonics were minimized by detuning the double crystal monochromator to 75% of the maximum.

III. BACKGROUND SUBTRACTION

A new background-subtraction method[9] was used for the data processing. It uses as a criterion of good background removal the optimization of the low r portion of the XAFS, Fourier transformed to r space. The normalized XAFS so obtained is

$$\chi(k) = \frac{\mu(k) - \mu_0(k)}{\Delta\mu_0(0)}, \quad (1)$$

where k is the wave number, $\mu(k)$ is the measured absorption, $\mu_0(k)$ is the background, and $\Delta\mu_0(0)$ is the edge jump.

Table I shows the values of parameters we used in the background subtraction. It contains an E_0, which is a variable determined by the fit, and fixed input values of $k_{\min}$ and $k_{\max}$, the lowest and highest limits of k, Δk, the region where the window function is reduced to zero with a Hanning function variation, $r_{\min}$, and r_1, the r range of the first peak, within which the theoretical χ_{th} function is fitted to data, and k^w the weighting parameter.

An accurate background function, corresponding to the absorption of an isolated atom, should reveal the presence of any multielectron excitations,[10,11] known as shake-up or shake-off processes. The reasonableness of this background-subtraction method is illustrated by the fact that it is consistent with such structure in our background functions for the Rb and Br edges of RbBr (Fig. 1). One can estimate the multielectron transition energy using the $Z+1$ rule (see, e.g., Ref. 11), which states that the excitation energy required to eject a second outer shell core level electron from an x-ray-absorbing atom with atomic number Z is equal to the binding energy of the same shell of an atom with atomic number $Z+1$. We therefore can estimate the energy of multielectron transitions in Br and Rb atoms from the binding energies of Kr and Sr, respectively. The binding energy of the $3d$ state in Kr and Sr is 95 and 135 eV,[12] respectively, which predicts the onset of the two-electron excitation of the $1s$ and $3d$ states to occur at those energies past the K edge for Br and Rb. Comparing these energies, shown by the arrows in Fig. 1, with the Rb and Br edge background functions of RbBr we can note that structure in the background functions corresponds to the $1s$ and $3d$ two-electron excitation energies.

IV. FITTING THEORY TO DATA

The XAFS data processing starts with the values of the average structure of the material which includes atom positions and types up to 10 Å around the core hole. The lattice of RbBr, RbCl, and KBr at low temperature and normal pressure is a NaCl structure. Theoretical XAFS functions $\chi_{\text{th}}(k)$ were calculated for each material using the known structure.

Our FEFF5 analysis is based on the curved-wave MS

TABLE I. Background-subtraction parameters for RbBr, RbCl, and KBr.

Salt	T (K)	E_0 (eV)	$k_{\min}$ (Å^{-1})	$k_{\max}$ (Å^{-1})	Δk (Å^{-1})	$r_{\min}$ (Å)	r_1 (Å)	k^w
RbBr (Rb edge)	30	15239	1.8	15.6	0.05	2	4	k
RbBr (Br edge)	30	13499	1.9	15.6	0.2	2	4	k
RbBr (Rb edge)	125	15240	1.8	15.6	0.2	2	4	k
RbCl (Rb edge)	30	15237	1.8	15.6	0.2	1.7	4	k
KBr (Br edge)	30	13500	1.8	15.6	0.05	1.6	3	k

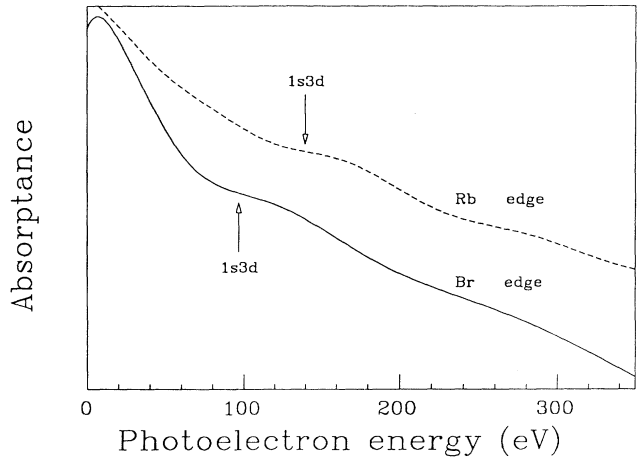

FIG. 1. The extracted XAFS background for the Rb and Br K edges of RbBr. Arrows indicate the energy of $1s, 3d$ two-electron excitations.

XAFS formula[2] for an N-leg ($N \geq 2$) path Γ with scatterers at $\mathbf{R}_1, \mathbf{R}_2, \ldots, \mathbf{R}_N$:

$$\chi_\Gamma(k) = \mathrm{Im}\ S_0^2 \frac{e^{i(\rho_1+\rho_2+\cdots+\rho_N+2\delta_l)}}{\rho_1\rho_2\cdots\rho_N} e^{-\sigma_\Gamma^2 k^2/2} \times \mathrm{Tr}\ MF^N \cdots F^2F^1. \quad (2)$$

Here $\boldsymbol{\rho}_i = k(\mathbf{R}_i - \mathbf{R}_{i-1}), k = \sqrt{2m(E-E_0)}$, E_0 is the photon energy, δ_l is the phase shift at the absorbing atom, F^i is the scattering matrix at site i, M is the $l = 1$ termination matrix, S_0^2 is a many-body reduction factor, and σ^2 is the mean-square variation in total path length.

The fitting of a theoretical XAFS function to the experimental signal is done in r space and usually may be performed relatively easy for the first single-scattering path. The fitting algorithm of the computer code FEFFIT[13] is based on a standard nonlinear least squares technique which minimizes the difference between the Fourier transformed XAFS signal and the theoretically summed paths of Eq. (2). To avoid unnecessary computations, not all possible paths are retained, only the significant ones. The default presorting criterion for retaining a path is that the amplitude of the contribution of a given path, estimated in the plane wave approximation, is above 2.5% of the first shell amplitude. The number of independent parameters which may be determined with XAFS is limited by N, the number of relevant independent data points,

$$N \approx \frac{2}{\pi}\Delta k \Delta R, \quad (3)$$

where Δk and ΔR are, respectively, the ranges in k and R space over which the data are fitted.

Table II contains $k_{\min}$, $k_{\max}$, $r_{\min}$, $r_{\max}$, and weighting parameter k^w, which were used for the Fourier transform of $\chi(k)$ to r space; N, the number of relevant independent points in the fitting range; and P, the number of fitting parameters used.

In our case the following parameters of each path were either fixed or allowed to vary: ΔE_Γ [shift of the energy origin in expression for k in Eq. (2)], S_0^2 (passive electrons reduction factor),[14] and the first three cumulants[14,15] in the k expansion of phase and amplitude of Eq. (2) for the first two shells and the first two cumulants for the rest of the shells. The first cumulant is ΔR (linear phase shift), second is σ^2 (Debye-Waller factor), and third is $c^{(3)}$ (cubic phase shift).

Among the parameters of $\chi_1(k)$, found from the fit to the first path, is S_0^2 which is averaged for a given center atom over all samples and then fixed for all further paths. The values of S_0^2 are fixed to be 0.98 for the Rb edge data (RbBr: $S_0^2 = 1.00$; RbCl: $S_0^2 = 0.96$) and 0.91 for the Br edge (RbBr: $S_0^2 = 0.89$; KBr: $S_0^2 = 0.93$).

The next parameter, ΔR_i, the shift of an average bond distance from the crystal structure value, is a measure of either noise in the data or errors in FEFF5. It can be used also when the bond distance may change under a phase transition or thermal expansion (contraction). In our case we usually assumed that the ΔR_i for each shell is related by the crystal structure to changes in the lattice constant Δa which decreases the number of independent parameters to only 1. The lattice parameters of the alkali halides for the theoretical XAFS calculation were corrected to low temperatures by thermal-expansion data.[16] The ΔR_1 (and, hence, ΔR_i for all paths involved) was found to be zero when the fit was optimized. All ΔR_i were then fixed to zero. If FEFF5 were perfect or there were no noise, that would be the end of the story. However, if FEFF5 theory had errors or there were noise, then this may be reflected by ΔR_i not really varying as the crystal structure predicts. We checked this in some cases and indeed obtained a better fit of theory to the data by varying each ΔR_i ($i \neq 1$) independently. The values of such ΔR_i were $\cong 0.01$ Å, which gives an uncertainty for ΔR_i of ± 0.01 Å.

In order to optimize the fit of theory to the data we also varied σ_i^2 for each path. The initial guess for σ_i^2 is taken from values calculated by the correlated Debye model and fitted by varying ΔE_Γ . The final values of σ_i^2 are found by next making them variables and fixing ΔE_Γ. The results were close to the initial guess values, giving confidence in them.

TABLE II. Fitting ranges for RbBr, RbCl, and KBr.

Salt	T (K)	$k_{\min}$ (Å^{-1})	$k_{\max}$ (Å^{-1})	$r_{\min}$ (Å)	$r_{\max}$ (Å)	k^w	N	P
RbBr (Rb edge)	30	2.5	12	2	10	k	48	14
RbBr (Br edge)	30	2.8	11	2	10	k	41	11
RbBr (Rb edge)	125	3	11	2	10	k	40	14
RbCl (Rb edge)	30	2.5	11	2	8	k	32	14
KBr (Br edge)	30	2.8	11	2	10	k	41	16

V. FIT RESULTS

Figure 2(a) gives the result of the preliminary fit given by the correlated Debye model to data of RbBr at 30 K (for Rb edge data), only ΔE_0 being varied. The poor quality of this preliminary fit at large r will be discussed later since it gives interesting physics, and we will show how it can be improved by considering the analysis of KBr and RbCl data. Figures 2(b) and 2(c) show the results of a final fit obtained by FEFF5 to experimental data of RbBr at 30 K and 125 K, respectively. In all cases, the R-space transform is with a k weighting of 1 and the k range as listed in Table II. We discuss the fit for the 30 K data since the 125 K data were fitted in the same way with the same paths.

The first peak (2.5–3.5 Å) corresponds to the nearest neighbor single-scattering (SS) path $c \rightarrow 1\text{NN} \rightarrow c$, where c is central atom (Rb, absorber) and 1NN is the first nearest neighbor (Br). The Debye-Waller factor of this path, σ^2, determined from the fit, is equal to $(5.5 \pm 0.4) \times 10^{-3}$ Å^2, while the initial guess of this value, obtained from the correlated Debye model, is 5.3×10^{-3} Å^2. The error in σ^2 is obtained from the variations given by either fitting theory to two independent measurements at the same temperature, or 0.5×10^{-3} Å^2, whichever is larger. The latter value is our estimate of systematic errors.

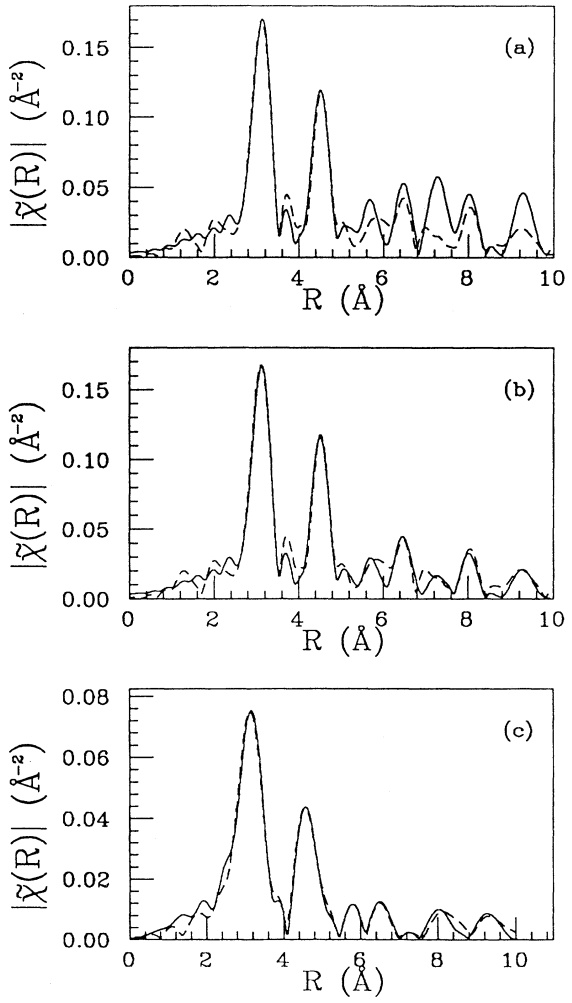

FIG. 2. (a) Fourier transformed Rb edge XAFS functions of RbBr data at 30 K and theoretical fit using correlated Debye model with overall ΔE_0 used. Final fit of FEFF5 theory to data at (b) 30 K and (c) 125 K by varying σ_i^2: dashed line, experiment; solid line, theory.

The next peak (2.5–3.5 Å) is contributed mostly by the second nearest neighbor 2NN SS path $c \rightarrow 2\text{NN} \rightarrow c$. It has contributions also from the distribution at larger values of R than the first peak and from smaller R values, corresponding to third nearest neighbor 3NN SS path $c \rightarrow 3\text{NN} \rightarrow c$, centered at 5 Å.

The analysis in the higher r range, especially in 5.5–10 Å, tests the reliability of FEFF5 in that range. The simple cubic lattice of our salts turned out to have only 13 significant paths out of the total hundreds of thousands of possible paths with half path length $\leq$ 10 Å. All the other paths are found to be insignificantly small. The significant paths are only SS and collinear focusing paths, both double-scattering (DS) and triple-scattering (TS) ones. This result is consistent with previous experiments[17] and theory.[18] Forward scatterings enhance the collinear DS and TS paths. On the other hand, many of the triangular double-scattering and rectangular triple-scattering paths are negligibly small because of the right angle between the initial and final legs of most of these paths.[17] In particular, the two peaks (Fig. 2) within 5.5–7 Å are dominated by the focusing paths: DS path $c \rightarrow 1\text{NN} \rightarrow 4\text{NN} \rightarrow c$ (and its time reversal path), TS path $c \rightarrow 1\text{NN} \rightarrow 4\text{NN} \rightarrow 1\text{NN} \rightarrow c$, and SS path $c \rightarrow 4\text{NN} \rightarrow c$, where 4NN is the fourth nearest neighbor. As a result of the fit we obtained [and it follows from the Eq. (2) as well], the focusing TS path makes a larger contribution to $\tilde{\chi}(R)$ than DS since it has two contributions from the forward-scattering matrix F^i. As was also determined from the fit, the dominant components of $\tilde{\chi}(R)$ within 7–8.5 Å are two SS paths $c \rightarrow 5\text{NN} \rightarrow c$ and $c \rightarrow 6\text{NN} \rightarrow c$, while the last investigated range 8.5–10 Å is dominated by the focusing paths: DS path $c \rightarrow 2\text{NN} \rightarrow 7\text{NN} \rightarrow c$ (and its time reversal path), TS path $c \rightarrow 2\text{NN} \rightarrow 7\text{NN} \rightarrow 2\text{NN} \rightarrow c$, and SS path $c \rightarrow 7\text{NN} \rightarrow c$.

Not all the adjustable variables of the Debye-Waller factors, σ_i^2, are independent; namely, the following relation holds to a good approximation: $\sigma_{\text{DS}}^2 = \sigma_{\text{TS}}^2 = \sigma_{\text{SS}}^2$ for the corresponding DS, TS, and SS paths, with the same half path length (Tables III–VII). The initial guess for the Debye-Waller factors of the MS paths was based on predicted values by the correlated Debye model.

Since our analysis includes all possible significant interactions between absorber and all its seven nearest neighbors we may conclude that the XAFS function $\chi(k)$ can be adequately fitted for RbBr up to 10 Å by only employing SS and focusing paths. This result is in agreement with the suggestion in Ref. 17.

We found ΔE_Γ to be an extremely important variable in our fit process. Using ionized-atom potentials in FEFF5 for the positive ion gives a sufficiently good approxima-

tion for the shift of the energy origin of a positive ion relative to a remote negative ion energy origin. We found that it was not necessary to use a negative ion potential for the negative ion because this would just change the relative E_0 shift, which is a variable parameter anyways. However, we found that it was necessary to add an additional ΔE_Γ to all of those paths that include scattering from first nearest neighbor. The physics of why this is necessary is that the core hole potential, if it is not well shielded (as expected in these salts), strongly perturbs the potential at its first neighbor site from approximate spherical symmetry. The muffin-tin potential, as FEFF5 assumes, would then be a bad approximation for this case, as well as having a different average value than the other shells. The ΔE_Γ necessary to correct this aspect of FEFF5 is ≈ 2.0 eV for the first shell SS and smaller for the MS paths that include the first shell. We find that the phase correction, introduced by this ΔE_Γ is big enough to significantly affect the fit.

In order to demonstrate the effect of this correction we will present the results of fit calculated with the standard procedure (a single ΔE_0 overall) and the modified method (different ΔE_Γ for paths containing nearest neighbors).

Figures 3 and 4 present fits of FEFF5 theory to 30 K data of KBr (Br edge) and RbCl (Rb edge), respectively. They demonstrate the influence of the different ΔE_Γ shifts, discussed above. Figures 3, 4(a), and 4(b) for both materials show the standard procedure (adjusting of ΔE_0 overall) and the modified fitting algorithm (different ΔE_Γ shifts), respectively, applied to fit the correlated Debye model to the data. Figures 3(c) and 4(c) give the final fit. In these two cases we find we need two more paths than in RbBr. Together with the same SS, focusing DS and TS paths used for RbBr we required also two other types of the DS and TS paths which have significant influence within 7.5–8 Å for both materials. These are the DS path $c \rightarrow 1\mathrm{NN} \rightarrow 1\mathrm{NN}' \rightarrow c$ and the

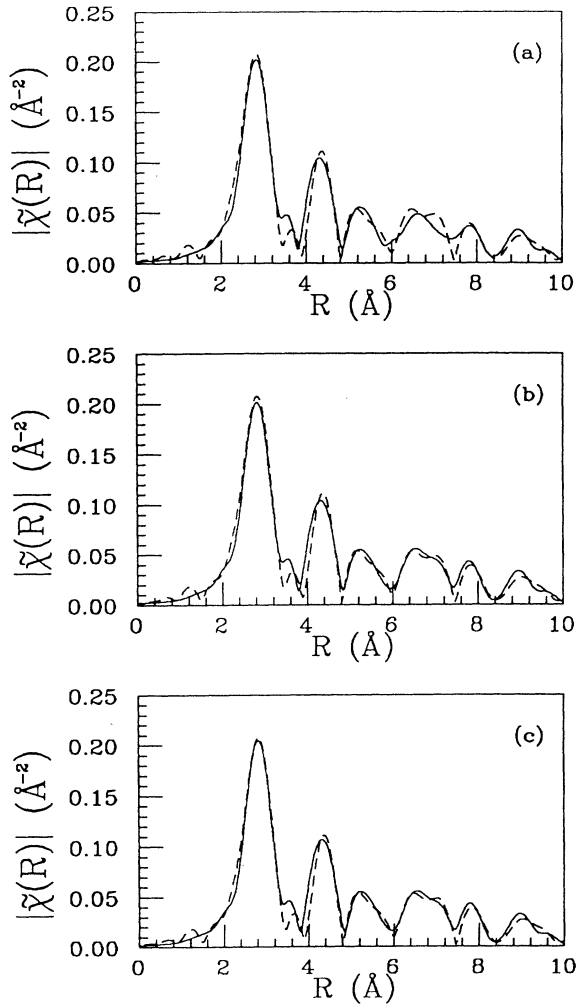

FIG. 3. Fourier transformed Br edge XAFS functions of KBr at 30 K: fitting of theory (correlated Debye model, solid line) to data (dashed line) by (a) adjusting ΔE_0 overall and (b) using ΔE_Γ for every path containing nearest neighbors; (c) final fit of FEFF5 theory to data by varying σ_i^2.

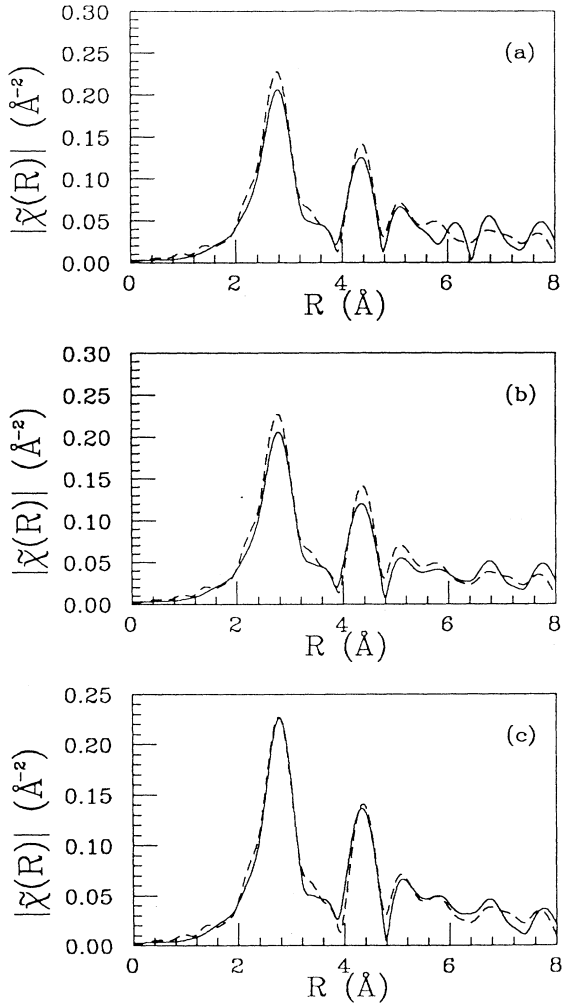

FIG. 4. Fourier transformed Rb edge XAFS functions of RbCl at 30 K: fitting of theory (correlated Debye model, solid line) to data (dashed line) by (a) adjusting ΔE_0 overall and (b) using ΔE_Γ for every path containing nearest neighbors; (c) final fit of FEFF5 theory to data by varying σ_i^2.

TABLE III. Path parameters of RbBr (Rb edge, 30 K) $\chi_{th}(k)$ for correlated Debye model (CDM) calculation and final fit; two left columns indicate path and half path length. Subscripts f and v indicate whether the given value was fixed in fitting process or allowed to vary, respectively.

Path Type	R (Å)	ΔE_Γ (eV) CDM	ΔE_Γ (eV) Final fit	σ^2 (10^{-2} Å^2) CDM	σ^2 (10^{-2} Å^2) Final fit
SS	3.41	1.3_v	1.3_f	0.53	$0.55_v \pm 0.05$
SS	4.82	-2.2_v	-2.2_f	0.68	$0.71_v \pm 0.05$
SS	5.90	-2.2_v	-2.2_f	0.74	$1.06_v \pm 0.05$
SS	6.81	-2.2_v	-2.2_f	0.71	$0.81_v \pm 0.05$
DS(Foc.: 1NN)	6.81	-1.1_v	-1.1_f	0.71	$0.81_v \pm 0.05$
TS(Foc.: 1NN)	6.81	-1.0_v	-1.0_f	0.71	$0.81_v \pm 0.05$
SS	7.61	-2.2_v	-2.2_f	0.73	$2.02_v \pm 0.05$
SS	8.34	-2.2_v	-2.2_f	0.71	$1.0_v \pm 0.1$

TS path $c \rightarrow 1NN \rightarrow c \rightarrow 1NN' \rightarrow c$, where 1NN and 1NN′ are the first nearest neighbors on opposite sides of the center atom. To decrease the number of fit variables we set $\sigma^2_{DS} = \sigma^2_{TS} = 2\sigma^2_1$, where σ^2_1 is the Debye-Waller factor of the 1NN bond.

It is seen from Figs. 3(a) and 4(a) that the biggest discrepancies between fit and data for the standard procedure are within 6–7.5 Å for KBr data and within 5.5–7 Å for RbCl data. We find that the poor fits in these r ranges are caused by four collinear MS paths, containing the first neighbor scattering which contributes in these ranges. By adding variable ΔE_Γ values to these paths the fit is improved in the region of interest as shown by Figs. 3(b) and 4(b).

Tables III, IV, V, VI, and VII present path parameters determined by our fits for RbBr (Rb edge, 30 K), RbBr (Br edge, 30 K), RbBr (Rb edge, 125 K), RbCl (Rb edge, 30 K), and KBr (Br edge, 30 K), respectively. The focusing (intervening) atom of the collinear DS and TS paths is shown in parentheses. The Br edge data of RbBr at 125 K were not analyzed past the first peak in r space since the two XAFS measurements were very noisy in the higher r range and the parameters of the paths, starting with the second (Br–Br bond), could not be determined with any accuracy.

The results are given both for the correlated Debye model (CDM) calculation (left column for each parameter) and for the final fit (right column) with σ_i^2 as a variable of the fit starting with values chosen from the CDM calculation.

TABLE IV. Path parameters of RbBr (Br edge, 30 K) $\chi_{th}(k)$ for correlated Debye model (CDM) calculation and final fit; two left columns indicate path and half path length. Subscripts f and v indicate whether the given value was fixed in fitting process or allowed to vary, respectively.

Path Type	R (Å)	ΔE_Γ (eV) CDM	ΔE_Γ (eV) Final fit	σ^2 (10^{-2} Å^2) CDM	σ^2 (10^{-2} Å^2) Final fit
SS	3.41	6.9_v	6.9_f	0.53	$0.54_v \pm 0.05$
SS	4.82	4.8_v	4.8_f	0.73	$0.73_v \pm 0.05$
SS	5.90	4.8_v	4.8_f	0.74	$1.1_v \pm 0.1$
SS	6.81	4.8_v	4.8_f	0.76	$0.77_v \pm 0.05$
DS(Foc.: 1NN)	6.81	5.3_v	5.3_f	0.76	$0.77_v \pm 0.05$
TS(Foc.: 1NN)	6.81	5.3_v	5.3_f	0.76	$0.77_v \pm 0.05$

TABLE V. Path parameters of RbBr (Rb edge, 125 K) $\chi_{th}(k)$ for correlated Debye model (CDM) calculation and final fit; two left columns indicate path and half path length. Subscripts f and v indicate whether the given value was fixed in fitting process or allowed to vary, respectively.

Path Type	R (Å)	ΔE_Γ (eV) CDM	ΔE_Γ (eV) Final fit	σ^2 (10^{-2} Å^2) CDM	σ^2 (10^{-2} Å^2) Final fit
SS	3.41	1.0_v	1.0_f	1.32	$1.05_v \pm 0.05$
SS	4.82	-2.2_v	-2.2_f	1.74	$1.58_v \pm 0.05$
SS	5.90	-2.2_v	-2.2_f	1.95	$1.92_v \pm 0.05$
SS	6.81	-2.2_v	-2.2_f	1.92	$1.92_v \pm 0.05$
DS(Foc.: 1NN)	6.81	-2.1_v	-2.1_f	1.92	$1.92_v \pm 0.05$
TS(Foc.: 1NN)	6.81	-2.3_v	-2.3_f	1.92	$1.92_v \pm 0.05$
SS	7.61	-2.2_v	-2.2_f	2.00	$4.80_v \pm 0.05$
SS	8.34	-2.2_v	-2.2_f	1.96	$2.10_v \pm 0.05$

VI. COLLINEAR SCATTERING AMPLITUDE OF Rb AND Br

In order to analyze the nature of the enhancement of forward-scattering paths, various calculations with FEFF5 were performed. We compared two DS focusing paths: Rb-Br-Rb (P_1) and Br-Rb-Br (P_2), where absorber and backscattering atoms are, respectively, Rb and Br and the forward-scattering atoms are the reverse. From the similarity of their electronic configurations (both Rb and Br deviate by one electron from the Kr structure and have close atomic numbers: $Z_{Rb} = 35, Z_{Br} = 37$) one could expect similar scattering properties of both atoms with respect to photoelectron wave and, hence, similar k dependences of total scattering amplitude for both paths. However, Fig. 5 shows a significant difference between two DS collinear scattering amplitudes, F_{P_1} and F_{P_2} for the paths P_1 and P_2, respectively. These differences are larger than just the percentage change of Z between the Br and Rb atoms. Amplitudes of F_{P_1} and F_{P_2} of Fig. 5 were calculated in the neutral atom model

TABLE VI. Path parameters of RbCl (30 K) $\chi_{th}(k)$ for correlated Debye model (CDM) calculation and final fit; two left columns indicate path and half path length. Subscripts f and v indicate whether the given value was fixed in fitting process or allowed to vary, respectively.

Path Type	R (Å)	ΔE_Γ (eV) CDM	ΔE_Γ (eV) Final fit	σ^2 (10^{-2}Å^2) CDM	σ^2 (10^{-2}Å^2) Final fit
SS	3.27	2.2_v	2.2_f	0.71	$0.55_v \pm 0.05$
SS	4.62	-0.3_v	-0.3_f	0.52	$0.40_v \pm 0.05$
SS	5.66	-0.3_v	-0.3_f	0.94	$0.55_v \pm 0.05$
SS	6.54	-0.3_v	-0.3_f	0.54	$0.44_v \pm 0.05$
DS(Foc.: c)	6.54	-0.6_v	-0.6_f	1.30	$1.1_v \pm 0.1$
TS(Foc.: c)	6.54	1.8_v	1.8_f	1.30	$1.1_v \pm 0.1$
DS(Foc.: 1NN)	6.54	1.4_v	1.4_f	0.54	$0.44_v \pm 0.05$
TS(Foc.: 1NN)	6.54	1.6_v	1.6_f	0.54	$0.44_v \pm 0.05$
SS	7.31	-0.3_v	-0.3_f	0.92	$1.20_v \pm 0.05$
SS	8.01	-0.3_v	-0.3_f	0.54	$0.80_v \pm 0.05$

TABLE VII. Path parameters of KBr (Br edge, 30 K) $\chi_{th}(k)$ for correlated Debye model (CDM) calculation and final fit; two left columns indicate path and half path length. Subscripts f and v indicate whether the given value was fixed in fitting process or allowed to vary, respectively.

Path Type	R (Å)	ΔE_Γ (eV) CDM	ΔE_Γ (eV) Final fit	σ^2 (10^{-2} Å^2) CDM	σ^2 (10^{-2} Å^2) Final fit
SS	3.27	2.0_v	2.0_f	0.64	$0.61_v \pm 0.05$
SS	4.62	1.6_v	1.6_f	0.54	$0.51_v \pm 0.05$
SS	5.66	1.6_v	1.6_f	0.87	$0.87_v \pm 0.05$
SS	6.53	1.6_v	1.6_f	0.56	$0.57_v \pm 0.05$
DS(Foc.: c)	6.53	1.6_v	1.6_f	1.15	$1.2_v \pm 0.1$
TS(Foc.: c)	6.53	1.6_v	1.6_f	1.15	$1.2_v \pm 0.1$
DS(Foc.: 1NN)	6.53	2.3_v	2.3_f	0.56	$0.57_v \pm 0.05$
TS(Foc.: 1NN)	6.53	1.2_v	1.2_f	0.56	$0.57_v \pm 0.05$
SS	7.30	1.6_v	1.6_f	0.85	$0.85_v \pm 0.05$
SS	8.00	1.6_v	1.6_f	0.55	$0.55_v \pm 0.05$

where all atoms are neutral. To understand the large difference, numerical experiments were performed to determine what are the most important factors to cause the difference between scattering amplitudes. First the Rb atoms were ionized in P_1 and compared in Fig. 6(a) with the original case Fig. 5 of neutral Rb atoms. Figure 6(b) shows the result for P_2 when the Rb atom is ionized as compared to the result when it is neutral. There is a change, but the change is smaller than the total change between P_1 and P_2 as shown in Fig. 5.

The total collinear scattering amplitude has contributions from both the forward-scattering amplitude of the focusing atom (1NN) and the backscattering amplitude of 4NN. Thus, it is incorrect to determine the forward-scattering amplitudes of the focusing Br and Rb atoms based on the calculation of the total amplitudes of paths Rb-Br-Rb and Br-Rb-Br since these paths have different backscatterers. We, however, may fix the backscattering atoms and calculate two imaginary paths: Rb-Rb-Rb and Br-Br-Br with FEFF5, using neutral atoms in all cases. The pairs of paths (a) Br-Rb-Br, Br-Br-Br and (b) Rb-Br-Rb, Rb-Rb-Rb have the same backscattering

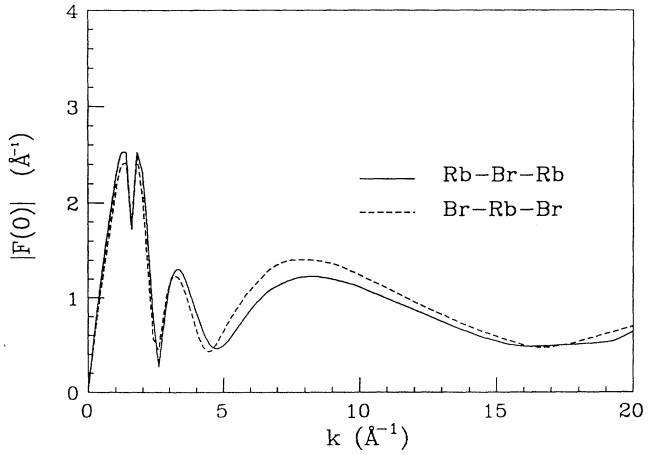

FIG. 5. Collinear scattering amplitude of DS focusing paths Rb-Br-Rb (solid line) and Br-Rb-Br (dashed line).

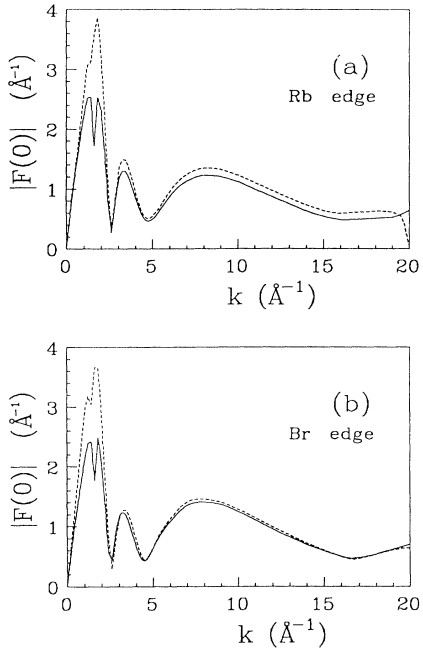

FIG. 6. Comparison of collinear scattering amplitudes of (a) Rb-Br-Rb and (b) Br-Rb-Br paths, as calculated from ionized atom model (dashed line) and neutral atom model (solid line).

atom and differ only in the type of focusing atom, allowing us to compare forward-scattering amplitudes from FEFF5. The results [Figs. 7(a) and 7(b)] demonstrate that in both cases when Rb was at the location of the focusing atom (solid lines) the collinear scattering amplitudes and, therefore, forward-scattering amplitudes were larger than those (dashed lines) of paths, containing Br as a focusing atom by an amount comparable to the difference found between P_1 and P_2, shown in Fig. 5. Since this change was not much affected whether the Rb was ionized or not, the enhanced increase in the focusing appears to be produced by the increased density of the Rb core compared to the negative Br ion, even though they have the same number of electrons.

VII. THERMAL-EXPANSION COEFFICIENT

In this section we apply the cumulant expansion method for determination of the thermal-expansion coefficient of RbBr. Stern *et al.*[14,19] found that within the classical limit $T \geq \Theta_D$ (Debye temperature), anharmonicity of atomic vibrations for Pb can be treated as a small perturbation and the linear thermal-expansion coefficient may be determined from the ratio

$$\alpha = \frac{c^{(3)}}{2R_0 T \sigma^2}, \tag{4}$$

where $c^{(3)}$ is the third cumulant, σ^2 is the Debye-Waller factor, and R_0 is the average interatomic distance. A similar result has been derived for the thermal expansion of surface atoms.[20]

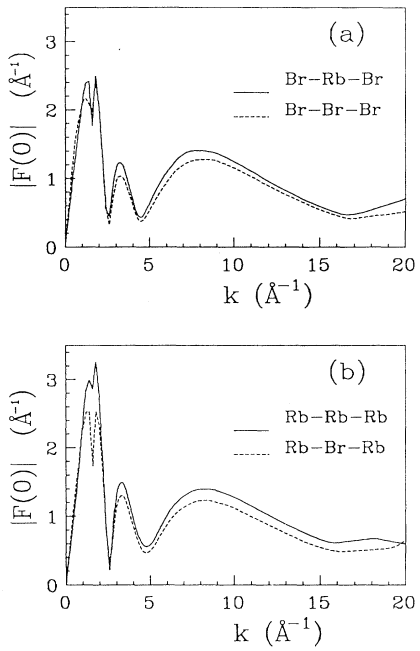

FIG. 7. Enhancement of F(0) for the paths containing Rb (solid) and Br (dash) as the forward-scattering atom. Absorber and backscattering atoms are the same and are Br (a) and Rb (b).

The second neighbor distance is the lattice constant of the RbBr crystal and its expansion should coincide with the expansion of the macroscopic sample. The first neighbor distance also should expand with the same α as the macroscopic value since the crystal retains its symmetry as it expands. Substituting the values of $c^{(3)}$ and σ^2 determined by XAFS (Table VIII) for the Rb–Br distance (first nearest neighbor, $R_0 = 3.41$ Å) and Rb–Rb distance (second neighbor, $R_0 = 4.82$ Å) at 125 K into Eq. (4) we find for the Rb edge data $\alpha = (2.9\pm0.3)\times10^{-5}$ K^{-1} and $\alpha = (3.1 \pm 0.3) \times 10^{-5}$ K^{-1}, respectively. As obtained from the Br edge data of RbBr at 125 K (Table VIII, Rb–Br bond) $\alpha = (2.7 \pm 0.4) \times 10^{-5}$ K^{-1}. The error bars are obtained using two different scans at any one temperature and third cumulant was found from the fit to each of them independently. Being close to the Debye temperature ($\Theta_D = 136$ K for RbBr), $T = 125$ K is high enough for the classical limit to be valid and thus agreement is expected between α calculated from the classical Eq. (4) and macroscopic experimental ones[16] ($\alpha = 3.0 \times 10^{-5}$ K^{-1}, $T = 125$ K). However the classical model cannot be used for the 30 K data and quantum corrections are needed. It has been shown[21] that for an anharmonic oscillator, including quantum effects,

$$\alpha = \frac{c^{(3)}}{R_0 T \sigma^2} \frac{3z(1+z)\ln(1/z)}{(1-z)(1+10z+z^2)}, \tag{5}$$

where $z = e^{-\frac{\hbar\omega}{k_B T}}$, ω is oscillation frequency, and k_B is Boltzmann constant. At very low temperatures ω can be found from the formula[21] for the zero point motion:

$$\sigma^2 \cong \frac{\hbar}{2\mu\omega}, \tag{6}$$

where the reduced mass $\mu = 1/(1/M_1 + 1/M_2)$. Table VIII contains the values of ω obtained for different bonds. At high temperature the values for ω were calculated independently using the classical formula[14,21]

$$\sigma^2 \cong \frac{k_B T}{\mu\omega^2}. \tag{7}$$

Substituting the values of low temperature cumulants σ_L^2 and $c_L^{(3)}$ (Table VIII) into Eq. (5) we obtain for the Rb–Br and Rb–Rb bonds (Rb edge data), at $T = 30$ K, $\alpha = (1.1\pm0.6)\times10^{-5}$ K^{-1} and $\alpha = (1.5\pm0.6)\times10^{-5}$ K^{-1}, respectively. The values for α found from the cumulants determined from the fit to the Br edge data (Table VIII) at 30 K for the Rb–Br and Br–Br bonds are consistent with the above Rb edge values: $\alpha = (1.0 \pm 0.6) \times 10^{-5}$ K^{-1} and $\alpha = (1.3 \pm 0.6) \times 10^{-5}$ K^{-1}, respectively. The experimental value[16] $\alpha = 1.0 \times 10^{-5}$ K^{-1} at $T = 30$ K.

Thus, the thermal-expansion coefficient as determined from XAFS cumulants satisfies macroscopic values in both the classical and quantum limits.

VIII. PHYSICAL CONSISTENCY OF THE RESULTS

The correctness of the results of the data analysis of several alkali halides (RbBr, RbCl, and KBr) at 30 K and 125 K can be checked by verifying that they satisfy consistency requirements imposed by the physics of the structure characteristics of the materials.

First, as it is predicted theoretically, the many-body relaxation factor S_0^2 [see Eq. (2)] is dependent only on the center atom and XAFS measurements of the different

TABLE VIII. Cumulants for the Rb–Br, Rb–Rb, and Br–Br bonds in RbBr from XAFS experiment at 30 K and 125 K.

T (K)	Absorber	Bond	ω (10^{13} Hz)	σ^2 (10^{-2} Å^2)	$c^{(3)}$ (10^{-4} Å^3)	α (10^{-5} K^{-1})
30	Rb	Rb–Br	1.4	0.55 ± 0.05	0.3 ± 0.2	1.1 ± 0.6
30	Rb	Rb–Rb	1.2	0.71 ± 0.05	0.5 ± 0.2	1.5 ± 0.6
30	Br	Rb–Br	1.4	0.54 ± 0.05	0.2 ± 0.1	1.0 ± 0.6
30	Br	Br–Br	1.1	0.73 ± 0.05	0.4 ± 0.2	1.3 ± 0.6
125	Rb	Rb–Br	1.5	1.05 ± 0.05	2.6 ± 0.3	2.9 ± 0.3
125	Rb	Rb–Rb	1.2	1.58 ± 0.05	6.5 ± 0.2	3.1 ± 0.3
125	Br	Rb–Br	1.6	1.00 ± 0.05	2.3 ± 0.4	2.7 ± 0.4

materials with the same absorbing atom should provide the same value of S_0^2. Indeed, in Sec. IV we report the close values of S_0^2 for Rb edge data. The S_0^2 values of the Br edge data are also found to be close to each other.

Second, the distribution of the relative displacements of any pair of atoms should be the same, regardless of which atom is the center atom. For example, in RbBr XAFS measurements about the Rb K edge and about the Br K edge should give the same R, σ^2, and $c^{(3)}$ for all Rb–Br distances, in particular, the first and third neighbors. Indeed, the final fit (Tables III and IV) provides σ^2 of c–1NN and c–3NN bonds to be the same for Br edge and Rb edge data. Table VIII shows that the values of $c^{(3)}$ for the shortest Rb–Br bond are within uncertainties for both the Rb edge and Br edge data of RbBr at both low and high temperatures.

Third, since the structure of the alkali halides expands uniformly with temperature, the thermal-expansion coefficient α must be the same for all pairs of atoms. As discussed in the previus section, this is the case for the first two nearest neighbors.

Fourth, the variation of σ^2 should follow that expected for a harmonic oscillator at low temperatures, with a temperature dependence consistent with its zero point motion. In our case, we obtain excellent agreement with an Einstein oscillator as attested to the fact that the oscillation frequencies obtained independently at low and high temperatures with Eqs. (6) and (7), respectively, are found to be equal within the error bars. For the Rb–Rb bond we get $\omega = (1.0 \pm 0.1) \times 10^{13}$ Hz at 30 K and $\omega = (1.2 \pm 0.1) \times 10^{13}$ Hz at 125 K. For the Rb–Br bond we obtain $\omega = (1.4 \pm 0.1) \times 10^{13}$ Hz (both from the Rb and Br edge data) at 30 K, $\omega = (1.5 \pm 0.1) \times 10^{13}$ Hz, and $\omega = (1.6 \pm 0.1) \times 10^{13}$ Hz at 125 K (Rb and Br edge data, respectively).

Fifth, in the collinear scattering case, where the intervening atom is a first nearest neighbor, this atom, to a good approximation, does not affect the σ^2 of these paths and they have the same values as the SS path of the same length. We set that condition and assigned the same σ^2 to the collinear DS (Foc.: 1NN) and TS (Foc.: 1NN) paths and decreased the number of variable parameters in the fit process. The notation in parentheses above indicates that the intervening (focusing) atom is a 1NN. In the other collinear scattering paths DS (Foc.: c) and TS (Foc.: c), where the intervening atom is a center atom, the σ^2 of these paths was set to twice the σ_1^2 value of the 1NN bond. Our excellent fit attested to the correctness of these conditions.

IX. SUMMARY AND CONCLUSIONS

Methods of XAFS data analysis were tested against XAFS measurements of RbBr, RbCl, and KBr at 30 K and 125 K.

An accurate background-subtraction method revealed the $1s, 3d$ two-electron photoexcitation as a step structure to the background function at the expected energy above the edge.

The multiple-scattering XAFS theory used in the computer code FEFF5, based on a curved-wave calculation of the photoelectron propagator, required several correction parameters, namely, an S_0^2 (≈ 0.8–1.0) normalization to correct for the passive electrons, an overall E_0 shift of the order of 1 eV to correct the Fermi energy, and an additional ΔE_0 shift of the order of 1 eV to all of the paths containing the first shell atoms to correct for the inadequacy of the muffin-tin potential at the first shell. With these corrections FEFF5 allowed us to extend the determination of accurate thermal disorder information up to 10 Å from the central atom. Second and third cumulants were determined for the first two neighbors and used to calculate thermal-expansion coefficients for RbBr at both 30 K and 125 K, using the quantum anharmonic Einstein model. Excellent agreement with macroscopic measurements of this coefficient was found.

It should be emphasized that the ability to obtain structural thermal disorder information to 10 Å or beyond is possible only because the average structure is known. If the average structure is not known, then to obtain this information plus the disorder about the average is possible only to about the first four neighbors.[6]

In the case of the NaCl structures we investigated we found that the only important scattering paths were single-scattering ones and the only those multiple-scattering paths that are collinear. This result is not a general one but is a consequence of the K edge and of that special feature of the NaCl structure where the bonds to the first neighbors to the center atom are perpendicular to one another. Under such circumstances, in double scattering among the first neighbors to the center atom, the emitted p wave does not overlap with the final p wave since they are oriented perpendicular to one another.[17] Normally, this double scattering is expected to be the largest noncollinear multiple-scattering contribution, but because of the geometry just discussed, its contribution is zero. The other feature that tends to decrease all the other multiple-scattering contributions is the comparatively large lattice constant.[17]

The influence of the focusing atom on the double collinear scattering amplitude was investigated by numerical calculations. The replacement of Rb by Br in the focusing atom site produced a larger increase in the forward-scattering amplitude than just the relative change in their Z values. Since this change was not much affected whether the Rb was ionized or not, the enhanced increase in the focusing appears to be produced by the increased density of the Rb core.

ACKNOWLEDGMENTS

This work was supported in part by DOE Grant No. DE-FG06-90ER45425 and by U.S.–Israel BNSF Grant No. 90-00152/1. Beamline X11A is supported by DOE Grant No. DE-FG05-89ER45384. One of us (A.I.F.) acknowledges the hospitality of the XAFS laboratory at the University of Washington where this work was carried out and we all wish to thank B. Ravel, S. Zabinsky, and Professor J. J. Rehr for stimulating discussions.

[1] J. J. Rehr, J. Mustre de Leon, S. I. Zabinsky, and R. C. Albers, J. Am. Chem. Soc. **113**, 5135 (1991); J. Mustre de Leon, J. J. Rehr, S. I. Zabinsky, and R. C. Albers, Phys. Rev. B **44**, 4146 (1991).
[2] J. J. Rehr, S. I. Zabinsky, and R. C. Albers, Phys. Rev. Lett. **69**, 3397 (1992).
[3] O. Hanske-Petitpierre, Y. Yacoby, J. Mustre de Leon, E. A. Stern, and J. J. Rehr, Phys. Rev. B **44**, 6700 (1991).
[4] B. Rechav, N. Sicron, Y. Yacoby, B. Ravel, M. Newville, and E. A. Stern, Physica C **209**, 55 (1993).
[5] B. Ravel, E. A. Stern, Y. Yacoby, and F. Dogan, Jpn. J. Appl. Phys. **32**, Suppl. 32-2, 782 (1993).
[6] E. A. Stern, Jpn. J. Appl. Phys. **32**, Suppl. 32-2, 851 (1993).
[7] E. A. Stern and K. Kim, Phys. Rev. B **23**, 3781 (1991).
[8] K. Q. Lu and E. A. Stern, Nucl. Instrum. Methods **212**, 475 (1983).
[9] M. Newville, P. Livins, Y. Yacoby, J. J. Rehr, and E. A. Stern, Phys. Rev. B **47**, 14126 (1993).
[10] G. Li, F. Bridges, and G. S. Brown, Phys. Rev. Lett. **68**, 1609 (1992).
[11] K. Zhang, E. A. Stern, J. J. Rehr, and F. Ellis, Phys. Rev. B **44**, 2030 (1991).
[12] *Handbook of Chemistry and Physics*, edited by R. C. Weast (CRC, Boca Raton, Florida, 1989), p. E-191.
[13] M. Newville (unpublished).
[14] E. A. Stern and S. M. Heald, in *Handbook on Synchrotron Radiation*, edited by E.-E. Koch (North-Holland, New York, 1983), Vol. 1, Chap. 10.
[15] E. D. Crozier, J. J. Rehr, and R. Ingalls, in *X-Ray Absorption: Principles, Applications, Techniques of EXAFS, SEXAFS and XANES,* edited by D. C. Koningsberger and R. Prins (John Wiley & Sons, New York, 1988), Chap. 9.
[16] G. K. White and J. G. Collins, Proc. R. Soc. London A **333**, 237 (1973).
[17] G. Bunker and E. A. Stern, Phys. Rev. Lett. **52**, 1990 (1985).
[18] P. A. Lee and J. B. Pendry, Phys. Rev. B **11**, 2795 (1975).
[19] E. A. Stern, P. Livins, and Zhe Zhang, Phys. Rev. B **43**, 8850 (1991).
[20] L. Wenzel *et al.,* Phys. Rev. Lett. **64**, 1765 (1990).
[21] A. I. Frenkel and J. J. Rehr, Phys. Rev. B **48**, 585 (1993).